Supporting Information

Sulfonyl passivation through synergistic hydrogen bonding and coordination interactions for efficient and stable perovskite solar cells

Yangyang Hao,‡ Xianzhao Wang,‡ Mingzhe Zhu, Xiafei Jiang, Long Wang, Guorui Cao,* Shuping Pang, and Zhongmin Zhou*

Experimental Section/Methods

Materials

All chemicals were purchased from commercial suppliers and used without further processing. The lead (II) iodide (PbI_2, 99.99%, TCI), Cesium Iodide (CsI, >99.0%, TCI) and lead (II) bromide ($PbBr_2$, >98%, TCI) were purchased from Beijing Innochem Science & Technology co., LTD. The methylammonium bromide (MABr), methylamine chloride (MACl), and formamidine iodide (FAI) were purchased from Xi'an Polymer Light Technology Corp. Super-dehydrated dimethylformamide (DMF, Acros), dimethyl sulfoxide (DMSO, Acros), ethyl ether (DE, Acros), chlorobenzene (CB, Acros), and isopropanol (IPA, Acros) were purchased from Beijing Innochem Science & Technology co., LTD.

Device fabrication

The FTO conductive substrate glass that has been etched needs to be cleaned with alkaline cleaning solution, deionized water, acetone, and isopropanol in an ultrasonic cleaning machine for 20 minutes, successively. Then the cleaned substrate was treated in an O_2 plasma cleaning machine for 5 min before use. A compact layer of TiO_2 was deposited atop FTO by atomic layer deposition and then sintered at 500℃ for 30 min in ambient air. SnO_2 colloid precursor was synthesized by $SnCl_4$ hydrolysis according to previously published work.[1] SnO_2 electron transport layer was obtained by spin-coating on the FTO/TiO_2 glass at 3000 rpm for 30 s, and then annealing for 30 min in an air atmosphere at 180 ℃. The perovskite solution was prepared by mixing 1.53 M PbI_2, 1.33 M FAI, 0.5 M MACl, 0.038 M MABr, 0.070 M CsI and 0.038 M $PbBr_2$ in mixed DMF/DMSO solvent system (v:v = 9:1). The precursor solution was firstly spin-coated at 1000 rpm for 10 s, then at 4000 rpm for 30 s, and 300 μL of the anti-solvent anisole was poured slowly at 20 s before the end of the second step. When preparing PSAD-treated devices, different concentrations of PSAD were pre-dissolved in the perovskite precursor solution. After the anti-solvent treatment, the devices were placed on a hot plate at 100 °C annealing for 40 min. Later, 40μL of 1mg/mL PTABr was evenly spread on the surface of the perovskite film and was spin-coated at 4000 rpm for 20 s. The spiro-OMeTAD solution, containing 72.3 mg spiro-OMeTAD, 28.8 μL 4-

tert-butyl pyridine, and 17.5 μL Li-TFSI solution (520 mg Li-TSFI in 1 mL ACN) in 1mL CB, was deposited on the perovskite film at a speed of 4000 rpm for 20 s after the perovskite film cooling to room temperature. Finally, the high-purity gold particles were vapor-deposited onto the surface of the Spiro-OMeTAD at an evaporation rate of 0.1-0.7 Å/s using a vacuum evaporation apparatus, and the thickness of the gold electrode was 80 nm.

Characterization

Top-view scanning electron microscope (SEM) images were obtained with a field-emission scanning electron microscope (S-4800, Hitachi). XRD patterns were measured by Ultima IV of Rigaku with Cu Kα radiation (1.5406Å). Nuclear magnetic resonance (NMR) spectra were recorded on 400 MHz or 500 MHz Bruker AVANCE III 600 NMR spectrometer in DMSO-d_6 or $CDCl_3$. Chemical shifts were reported in parts per million (δ) relative to tetramethylsilane (TMS). Fourier transform infrared (FTIR) spectroscopy characterization was performed by a Nicolet iS50 (Thermo Scientific) under purging with nitrogen gas. Silicon substrates were used for FTIR measurements. X-ray photoelectron spectroscopy (XPS) spectra analysis of films on ITO was performed in the air using a Thermo Fisher ESCALAB 250 Xi. Curve fitting was performed using the Thermo Avantage software. The curves were corrected based on the C1s peak at 284.8 eV. The UV-vis absorbance was measured by UV/Vis spectrometer (Ocean Optics). Steady PL was recorded on a fluorometer (Ocean Optics) excited at 460 nm. Time-resolved PL was determined with the single-photon counting technique using an Edinburgh F900 spectrometer with an excitation wavelength at 460 nm. An electrochemical workstation (CHI660E) was used to measure Mott-Schottky C-V curves and electrochemical impedance spectroscopy (EIS) curves in the dark. The TPV curves were obtained using a homemade laser pulse oscilloscope. The UPS equipped with He-I source ($h\upsilon$ = 21.22 eV) (AXIS ULTRA DLD, Kratos, UK) was used to determine the valence band energy and Fermi level. The Fermi level of the samples was referred to as that of Au which was in electrical contact with a sample in UPS measurements. The *J-V* characteristics of the devices (voltage scanning rate 10 mV/30 ms) and the steady photocurrent under maximum power output bias were

recorded under AM 1.5G illumination at 100 mW cm^{-2} with a solar simulator (Sumitomo Heavy Industries Advanced Machinery) under ambient conditions. *J-V* curves for all devices were measured by masking the devices with a metal mask with an aperture area of 0.09 cm^2. The light intensity of the solar simulator was calibrated with a standard silicon solar cell certified by the National Renewable Energy Laboratory. The EQE spectra were carried out using a Sciencetech SF150 xenon arc lamp and a PTI monochromator, with the monochromatic light intensity calibrated by a Si photodiode (Newport, 818-UV). All the measurements were carried out in an ambient atmosphere. Air Stability Test: Place all unsealed cells in a dry box at ambient with a relative humidity of < 10%. Operational stability test: The MPP stability tests was performed using a stability setup (LC Auto-Test 24, Shenzhen Lancheng Technology Co., Ltd.). In the test, all PSCs were un-encapsulated, tested under continuous light illumination and maximum power point tracking (controlled and monitored to be 15 ^oC). The light source consisted of an array of white LEDs (MG-A200A-AE) powered by a constant current. Sun intensities were calibrated by a calibrated Si-reference cell. During aging, the devices were masked and placed in a holder purged with continuous N_2 flow. *J-V* curves with reverse voltage scans were recorded every 0.5 h during the whole operational test.

DFT calculations

The Structures were optimized under M06-2X/def2TZVP level by Gaussian 16 Rev A.03 and certified without any imaginary frequencies before calculations of complexation energy.[2] HOMO/LUMO information was derived from Multiwfn 3.8 dev bin Win64 and the molecular orbital isosurfaces were drawn by VMD 1.9.3.[3] The coordinates of atoms of doping molecule (PSAD), PSAD-FA^+, and PSAD-Pb^{2+} complexes were shown in Table S6-S8, respectively.

Synthetic details

Synthesis of 3-ethylbenzo[d]isothiazole 1,1-dioxide (PSAD)

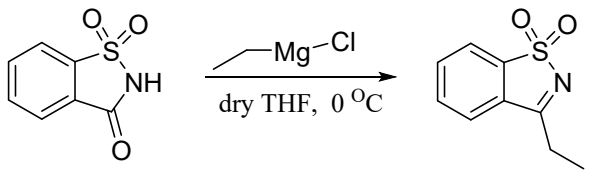

To a 100-mL three-necked flask, o-benzoylsulfonimide (10 mmol) was dissolved in 25 mL anhydrous tetrahydrofuran. The flask was placed in an ice bath to lower the temperature to 0 °C. Grignard reagent ethylmagnesium chloride (10 mL, 2 M) was added dropwise to the reaction system through a constant pressure dropping funnel, and the reaction temperature was gradually raised to room temperature and stirred overnight under argon protection. The reaction was quenched with saturated ammonium chloride solution, and extracted with ethyl acetate. The organic phases were combined, and dried over anhydrous sodium sulfate, then filtered with suction and rinsed the filter cake twice with ethyl acetate. The obtained filtrate was distilled under reduced pressure with a rotary evaporator to obtain a crude product, which was separated and purified by column chromatography (ethyl acetate : petroleum ether = 4:1) to obtain a white solid (1.54 g) with a yield of 78.9%.

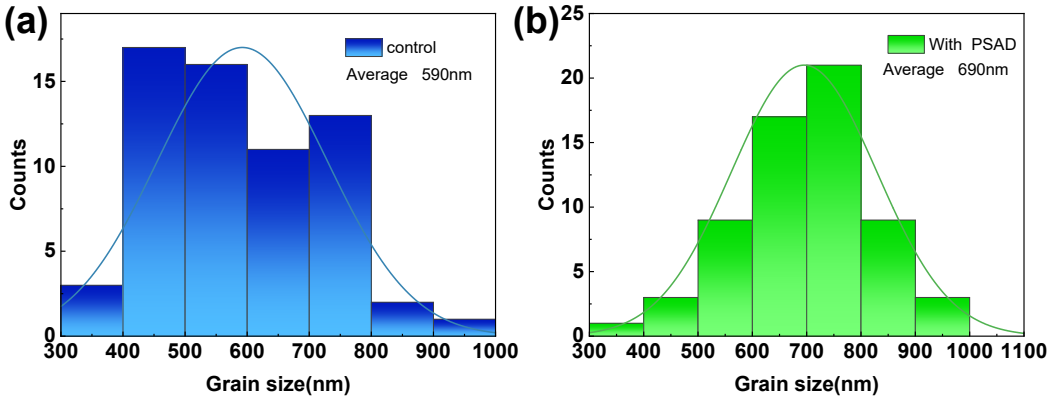

Figure S1. Statistics of grains size of perovskite films without (a) and with (b) PSAD treatment, respectively.

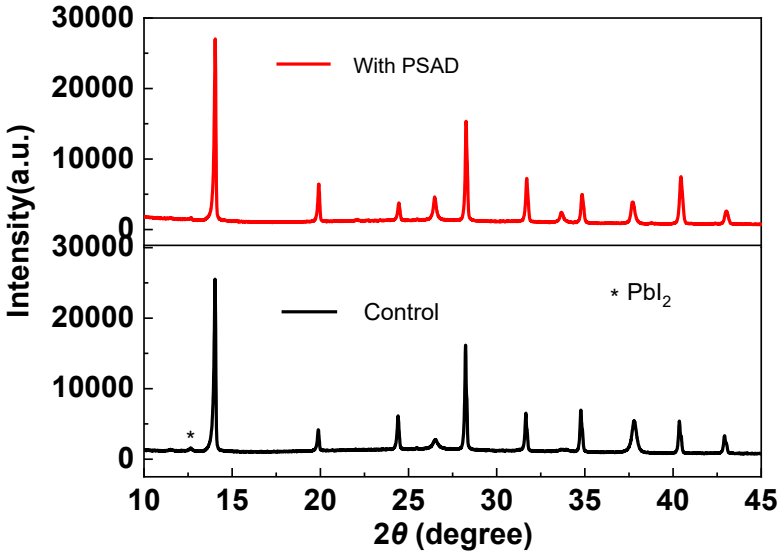

Figure S2. XRD patterns of the control film and perovskite film with PSAD.

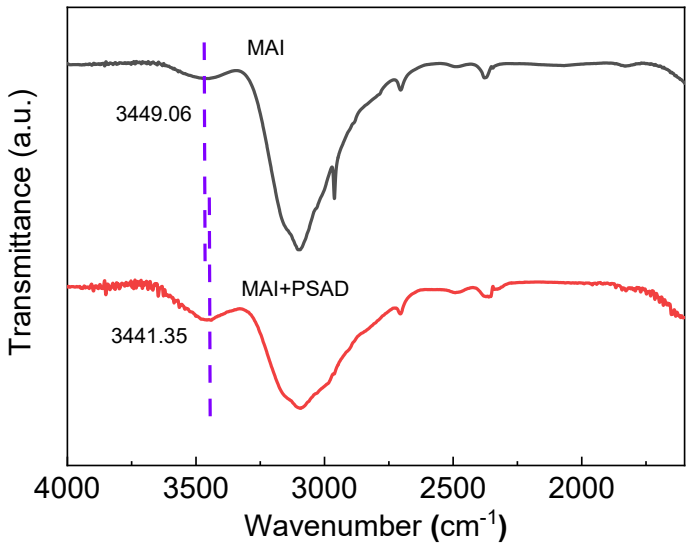

Figure S3. FTIR spectrum of MAI films with/without PSAD.

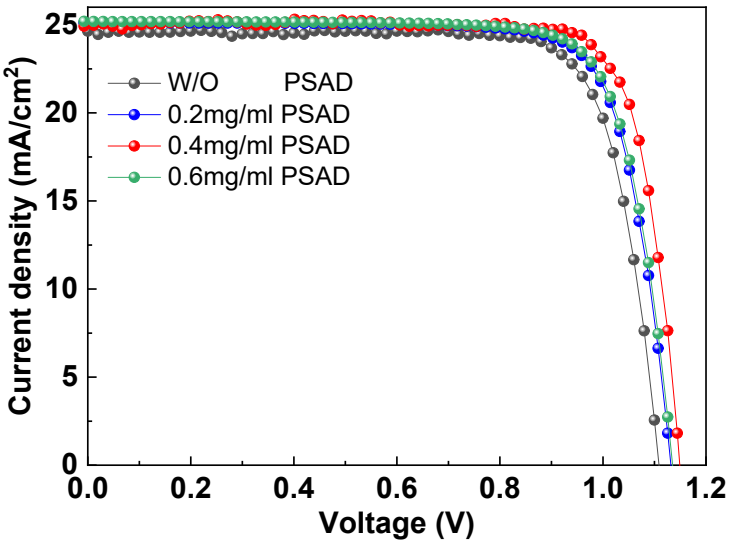

Figure S4. *J–V* characteristics of optimal devices based on perovskite films with different concentrations of PSAD.

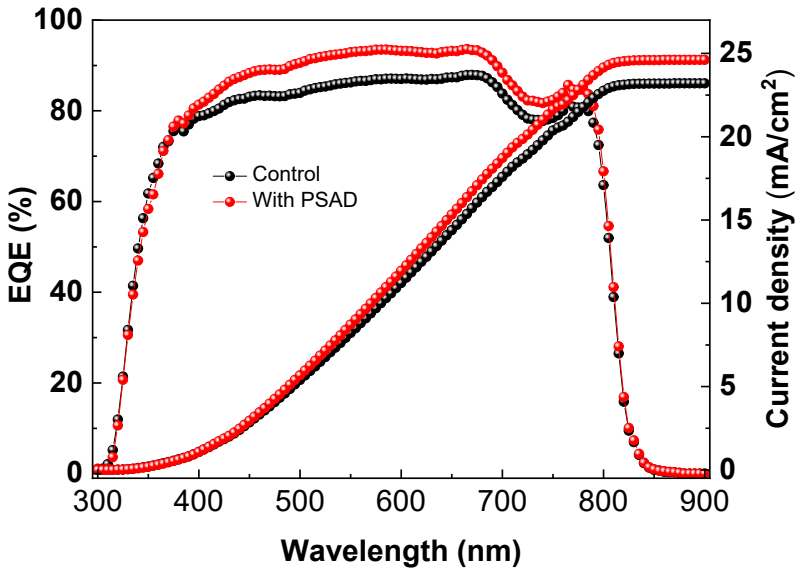

Figure S5. EQE spectrum of devices based on perovskite films with/without PSAD.

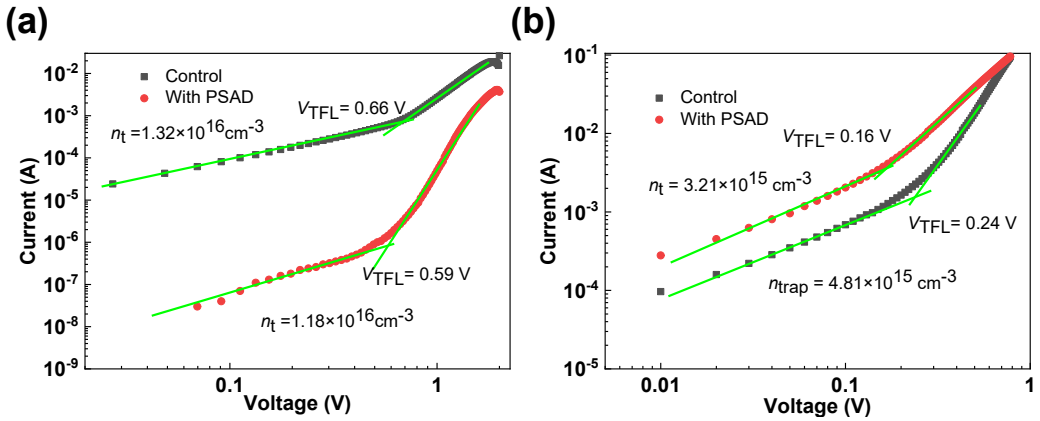

Figure S6. Dark current–voltage responses of electron-only (a) and hole-only (b) devices based on perovskite films with/without PSAD.

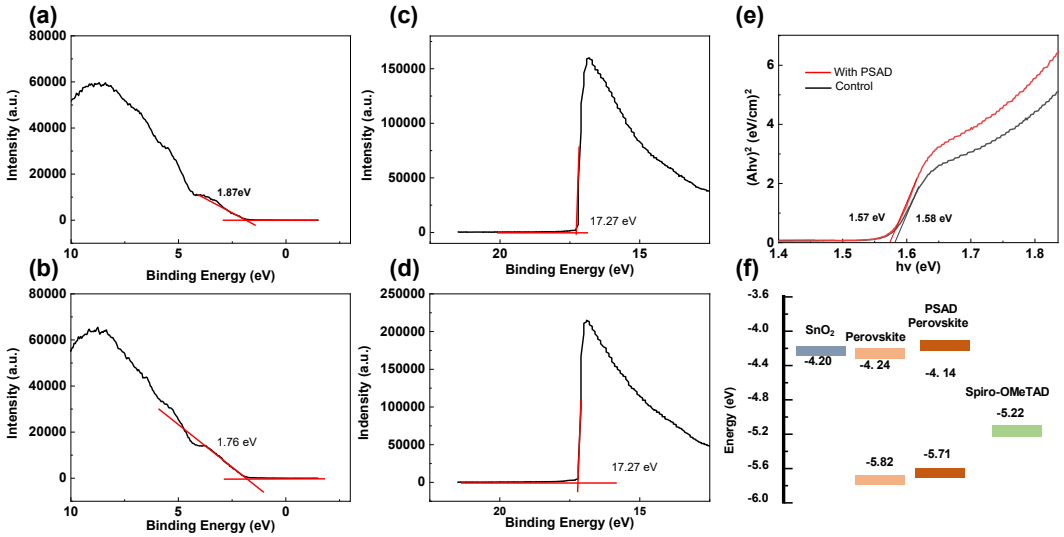

Figure S7. UPS spectra of the perovskite films without/with PSAD modification in the secondary-electron cut-off region (a) and (b), in Fermi edge region (c) and (d), respectively. (e) Energy-level diagram for the corresponding materials used in PSCs.

Table S1. Photovoltaic parameters of devices with different concentrations of PSAD.

Sample	*V*oc [V]	*J*sc [mA/cm^{-2}]	FF	PCE [%]
W/O PSAD	1.108	24.62	0.787	21.46
0.2mg/ml PSAD	1.131	25.11	0.784	22.29
0.4mg/ml PSAD	1.153	25.33	0.816	23.85
0.6mg/ml PSAD	1.145	24.52	0.788	22.13

Table S2. Photovoltaic parameters of devices with PSAD passivation.

Sample	*Voc*[V]	*Jsc*[mA/cm^{-2}]	FF	PCE[%]
With PSAD	1.153	25.33	0.816	23.85
	1.143	25.15	0.809	23.26
	1.149	25.66	0.780	22.98
	1.151	25.82	0.783	23.27
	1.149	25.15	0.783	22.60
	1.146	25.19	0.788	22.74
	1.157	24.79	0.791	22.70
	1.154	24.79	0.790	22.59
	1.153	24.87	0.787	22.58
	1.148	25.01	0.812	23.33
	1.140	24.85	0.793	22.45
	1.142	25.26	0.802	23.16
	1.146	24.76	0.789	22.39
	1.153	25.22	0.778	22.61
	1.153	25.85	0.747	22.25
	1.151	25.52	0.767	22.54
	1.150	25.66	0.780	23.02
	1.153	25.41	0.768	22.51
	1.145	24.93	0.775	22.10
	1.151	24.57	0.786	22.24

Table S3. Photovoltaic parameters of control devices.

Sample	*Voc*[V]	*Jsc*[mA/cm^{-2}]	FF	PCE[%]
Control	1.108	24.62	0.786	21.46
	1.096	23.91	0.763	19.99
	1.105	24.30	0.767	20.60
	1.104	24.48	0.790	21.33
	1.113	24.00	0.790	21.09
	1.115	24.10	0.793	21.32
	1.108	24.47	0.758	20.56
	1.094	24.78	0.745	20.19
	1.112	24.32	0.755	20.41
	1.107	23.25	0.757	20.31
	1.101	23.45	0.757	19.55
	1.091	24.25	0.730	19.31
	1.124	24.39	0.770	21.12
	1.121	24.50	0.765	21.02
	1.112	24.22	0.791	21.30
	1.121	24.42	0.772	21.13
	1.103	23.90	0.791	20.86
	1.121	23.97	0.793	21.31
	1.124	23.05	0.797	20.65
	1.126	24.11	0.780	21.17

Table S4. Parameters of the TRPL spectroscopy of perovskite films with/without PSAD.

Sample	τ_{ave} (ns)	τ_1 (ns)	τ_2 (ns)	A_1(ns)	A_2(ns)
Control	8.67	1.96	10.31	0.5621	0.4379
With PSAD	68.11	10.00	68.35	0.0274	0.9726

Table S5. Specific values of series resistance (R_s), charge transport resistance (R_{ct}) recombination resistance (R_{rec}) of PSCs without and with PSAD.

Sample	R_s (Ω)	R_{ct} (Ω)	CPE_1	R_{rec} (Ω)	CPE_2
Control	71.13	15277	1.2007E-08	21797	4.7244E-06
With PSAD	62.2	13810	1.384E-08	28062	2.5598E-06

Table S6. The Z-matrix and Cartesian coordinates of atoms of PSAD.

Symbol	Bond/Å	Angle/deg	Dihedral/deg	X/Å	Y/Å	Z/Å
C				-1.0264	-0.30778	0.00003
C	1.382442			-0.32927	0.886021	-2.2E-05
C	1.384522	120.1263		-1.01295	2.089968	-0.00002
C	1.391315	118.1473	-0.00174	-2.40382	2.054925	-2E-06
C	1.39089	120.9467	0.00079	-3.0888	0.844397	0.00003
C	1.376384	122.7498	0.002238	-2.40151	-0.36702	0.00004
C	1.492098	110.3846	180	1.140618	0.629526	-1.7E-05
H	1.082629	121.1904	179.9987	-0.48446	3.034844	-0.00004
H	1.081831	119.6099	-179.999	-2.96186	2.981718	-9E-06
H	1.081944	119.5377	-180	-4.17074	0.843751	0.000036
H	1.081738	121.414	179.9984	-2.92507	-1.31361	0.000055
N	1.275622	116.578	0	1.506746	-0.59242	0.00003
C	1.493673	121.1147	-179.998	2.120814	1.75659	-2.1E-05
H	1.095225	107.2413	-56.4566	1.897714	2.380828	-0.87184
H	1.095222	107.243	56.45028	1.897661	2.380919	0.871717
C	1.518898	113.9628	179.9972	3.572953	1.311231	0.000054
H	1.088902	110.6954	59.54505	3.789505	0.70475	-0.87801
H	1.088918	110.3057	179.9997	4.233671	2.176791	0.000042
H	1.088902	110.6952	-59.5459	3.789434	0.704829	0.878189
S	1.683041	110.8699	0.002958	0.172385	-1.61815	-6E-06
O	1.426235	108.8238	113.6353	0.137433	-2.32773	-1.2367
O	1.426236	108.8253	-113.645	0.137422	-2.32786	1.236618

Table S7. The Z-matrix and Cartesian coordinates of atoms of the ideal PSAD- FA^+ complex.

Symbol	Bond/Å	Angle/deg	Dihedral/deg	X/Å	Y/Å	Z/Å
C				0.981103	-1.037	-1.6E-05
C	1.385376			1.993349	-0.09115	0.000001
C	1.382724	119.8315		3.314871	-0.49797	0.000013
C	1.392841	118.0345	0	3.578821	-1.86557	0.000009
C	1.390145	121.1887	0	2.547572	-2.79779	-7E-06
C	1.375424	123.3166	0	1.213822	-2.39259	-2.1E-05
C	1.491667	110.7159	-180	1.426317	1.288541	0.000011
H	1.082257	121.2937	-180	4.124235	0.220507	0.000027
H	1.081601	119.4676	-180	4.604266	-2.20955	0.00002
H	1.08158	119.5748	-180	2.782365	-3.85358	-9E-06
H	1.081455	121.9647	180	0.406441	-3.11209	-3.3E-05
N	1.284203	116.1618	0	0.144967	1.374095	0.000006
C	1.487642	121.6186	-180	2.301559	2.491466	0.000028
H	1.095736	106.8496	-56.1113	2.961239	2.404259	0.870576
H	1.095735	106.8498	56.10956	2.961272	2.404263	-0.87049
C	1.518695	114.467	179.9992	1.553867	3.813355	0.000018
H	1.088839	110.838	59.91241	0.919115	3.899326	0.880512
H	1.088026	110.0075	-180	2.260468	4.64071	0.000028
H	1.08884	110.8378	-59.9121	0.919141	3.899325	-0.8805
S	1.655143	110.3302	-0.00027	-0.5322	-0.13618	-1.8E-05
O	1.441728	109.5132	116.1997	-1.27669	-0.33016	1.219283
O	1.441729	109.5131	-116.199	-1.27667	-0.33013	-1.21934
C	3.668008	101.4056	106.9563	-4.73034	-0.13034	0.00001
H	1.08415	160.5841	-169.638	-5.81241	-0.06319	0.000001
N	1.304388	81.66444	9.760851	-4.12416	-0.16815	-1.15435
H	1.025686	122.4092	-0.02191	-3.1036	-0.22775	-1.23766
H	1.007409	119.3964	-179.559	-4.66941	-0.13114	-2.00064
N	1.304389	42.83559	-170.545	-4.12419	-0.16828	1.15438
H	1.007411	119.3969	179.4442	-4.66945	-0.13137	2.000666
H	1.025682	122.4082	-0.09156	-3.10363	-0.22787	1.237684

Table S8. The Z-matrix and Cartesian coordinates of atoms of the ideal PSAD- Pb^{2+} complex.

Symbol	Bond/Å	Angle/deg	Dihedral/deg	X/Å	Y/Å	Z/Å
C				-1.83234	-1.0473	0.000355
C	1.396932			-2.92837	-0.18119	-0.00024
C	1.378219	119.2734		-4.20251	-0.7066	-0.00081
C	1.399633	118.0199	0	-4.33934	-2.09953	-0.00077
C	1.388554	121.569	0.001509	-3.23301	-2.93865	-0.00014
C	1.376747	124.0105	-0.00269	-1.93573	-2.42016	0.00047
C	1.488583	111.3309	179.9936	-2.4935	1.242457	-5.9E-05
H	1.082581	121.4259	179.999	-5.0765	-0.06776	-0.00127
H	1.082225	119.1772	179.9997	-5.3313	-2.53222	-0.0012
H	1.081829	119.7344	179.9983	-3.37318	-4.01136	-0.00009
H	1.081603	122.8741	-179.996	-1.07398	-3.07381	0.000999
N	1.307641	115.1863	0.003928	-1.19922	1.42897	0.000528
C	1.473887	123.0493	-179.994	-3.4402	2.372103	-0.00046
H	1.098915	106.1277	-55.2425	-4.09717	2.21949	-0.86805
H	1.098914	106.1276	55.23398	-4.09801	2.219409	0.866473
C	1.518716	115.5182	179.9953	-2.80998	3.753888	-8.5E-05
H	1.0888	111.0409	60.49772	-2.19202	3.90194	-0.88421
H	1.087329	109.4584	-179.999	-3.59247	4.508875	-0.00041
H	1.088801	111.0402	-60.4962	-2.19286	3.901827	0.884655
S	1.604489	109.3905	-0.00568	-0.4561	0.006946	0.001031
O	1.489239	111.0114	122.6041	0.455663	-0.11949	-1.16967
O	1.488961	111.0307	-122.639	0.455153	-0.11934	1.171789
Pb	2.332515	97.59888	110.3788	2.472231	-0.03805	-0.00029

Reference

[1] Z. Li, L. Wang, R. Liu, Y. Fan, H. Meng, Z. Shao, G. Cui, S. Pang, *Adv. Energy. Mater.* 2019, **9**, 1902142.

[2] Frisch, M. J.; Trucks, G. W.; Schlegel, H. B. et al. *Gaussian 09, Revision A.02, Gaussian Inc.,* Wallingford CT, 2016.

[3] T. Lu, F. Chen, *J. Comput. Chem.* 2012, **33**, 580–592.